Chinese Journal of Chemical Engineering, **16**(4) 558—563 (2008)

Numerical Investigation of Coupling Effect in Multipipe Ceramic Filter Vessel*

LI Haixia (李海霞)[1,2,**], **JI Zhongli** (姬忠礼)[1], **WU Xiaolin** (吴小林)[1] **and CHOI Joo-Hong** (崔柱洪)[3]
[1] Department of Mechanical and Electric Engineering, China University of Petroleum, Beijing 102249, China
[2] School of Mechanical and Power Engineering, Henan Polytechnic University, Jiaozuo 454000, China
[3] Department of Chemical Engineering, Gyeongsang National University, Jinju 660-701, Korea

Abstract The Reynolds stress transport model and the Eulerian two-fluid model provided by the FLUENT code were applied to evaluate the gas-particle two-phase flow in the ceramic filter vessel. The ceramic filter vessel contains six candle filters, which are arranged in the form of equilateral hexagon. The variation of the areal density of the filter cake during the filtration and the back-pulse process were analyzed. The coupling effect between filters, gas and solid, filtration and pulse cleaning process were investigated, respectively. The numerical results show a good approach to predict the particle distribution in the vessel and the particle deposition on the filter element. This study provides the base for the intensive study on the analysis of the gas-particle flow in the filter vessel.
Keywords multipipe ceramic filter vessel, gas/solid two-phase flow, numerical simulation

1 INTRODUCTION

The ceramic filter has been considered to be one of the most promising particle separation technology from gas at high temperature owing to its high filtration efficiency, heat-shock resistance, and gas erosion resistance [1−4]. There are many problems that threat the stability and the reliability of the filtration process [5−10], such as the bridging of dust cakes between adjacent filters due to the uneven particle removal [11, 12]. This leads to gradual increase of local particle layer thickness, and the particle bridge then occurs and damages the filters [13−17].

In this study, the computer simulation of gas flow and particle transport and deposition in the hot-gas filtration vessel is presented. To improve the reliability of the filtration system by overcoming the problem described above, numerical studies on the ceramic filters were carried out to investigate the couple effect between filters, gas and particle, filtration and pulse cleaning process, respectively.

2 CANDLE FILTER VESSEL GRID PARTITION

The filter vessel models the particle removal system for the coal gasification process and accommodates six ceramic filters which are arranged in the normal hexagon. In the present model, the filter is 6 cm in outer diameter and 1.5 m length. The aperture of porous film on the filter body is about 10−15 μm. The straight nozzle (6 mm in inner diameter) is located above the diffuser. The gap between the nozzle tip and the diffuser top is 50 mm. The schematic diagram of the filter vessel geometry and the measurement points are shown in Fig. 1. The inlet of the dusty gas is located at one side of the filter vessel in the position under 200 mm of the bottom of the filter element (the close end of the filter element). The origin of the coordinate system is set at the center of the section,

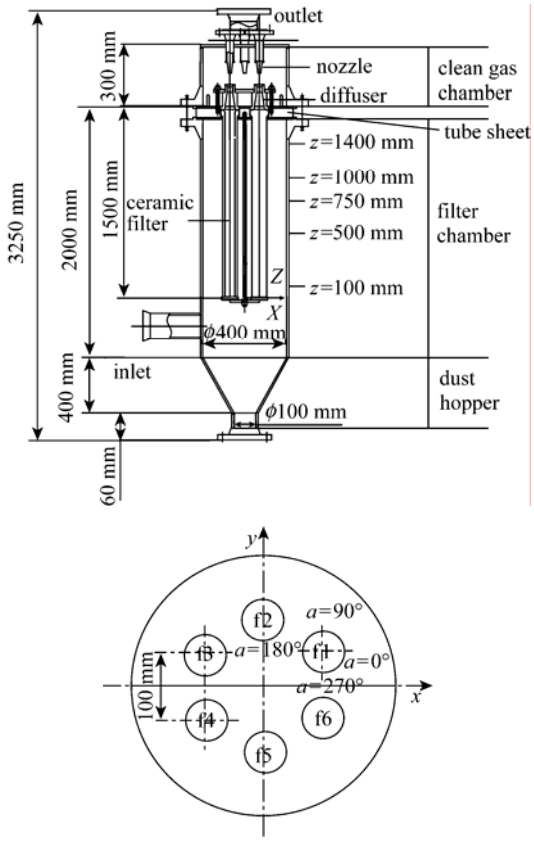

Figure 1 Schematic diagrams of filter vessel

which is on the same horizontal as the bottom of the filter element. The *z*-axis (the longitude coordination) starting from the close end of the filter element is contrary to the gravitational direction. The *x*-axis is along inlet flow direction. The positions of the measuring points are denoted with letter *a*, which represents counterclockwise angle between two lines that cross on the centre line of corresponding filter to be investigated.

Received 2007-07-30, accepted 2007-12-22.
* Supported by the National High Technology Research and Development Program of China (2007AA03Z524).
** To whom correspondence should be addressed. E-mail: lihx815@yahoo.com.cn

The initial line is parallel to the *x*-axis, and the final line passes through the measuring point. To identify the relative position of the filters, the six filters are named as f1, f2, f3, f4, f5, and f6 in counterclockwise.

Considering the big outline and the complex configuration of the filter vessel, the blend of structured and unstructured grid are used to simulate the flow field. To obtain the appropriate solution independent of grid, different grids are used to simulate the filtration gas flow in the filter vessel. The grid of 744653 cells is used which is shown in Fig. 2. Patankarhe gave the method of resistance distribution, namely the porous medium model to simulate flow field in the porous material. This method considers the effect of the solid structure on the fluid flow to be resistance added on the fluid. So, the fluid flow in the porous medium can be simulated with coarse grid [18].

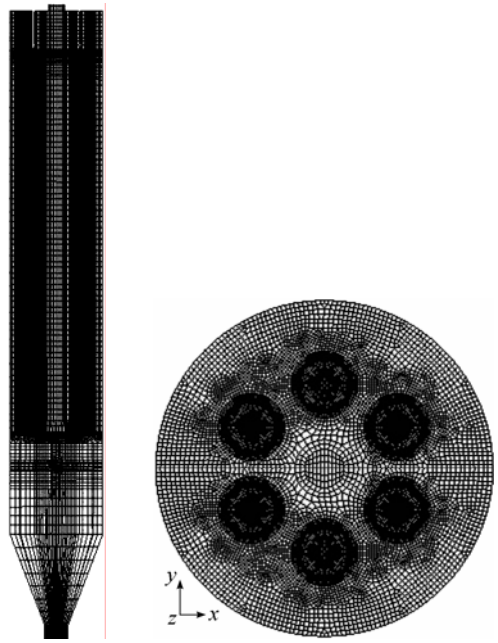

Figure 2 Schematic diagrams of grids of filter vessel

3 MODELS AND BOUNDARY CONDITIONS

The Reynolds stress transport model accounts for the evolutions of the individual stress components, and thus completely avoids the use of an eddy viscosity and is well suited for handling the anisotropic turbulence fluctuations. So, in this study, it is applied to simulate the gas flow in view of the flow condition during the pulse cleaning process where only two candle filters out of six are to be cleaned.

In the Eulerian approach, the two phases are considered to be separate interpenetrating continua and separate (but coupled) equations of motion with separate boundary conditions solved for each phase. Conservation equations for each phase are derived to obtain a set of equations, which have similar structure for all phases (Fluent User's Guide, Version 6.0).

The continuity equation for phase q is

$$\frac{\partial}{\partial t}\left(\alpha_q\rho_q\right)+\nabla\cdot\left(\alpha_q\rho_q\boldsymbol{u}_q\right)=0 \tag{1}$$

where α_q, ρ_q, and $\boldsymbol{u}_q$ are the volume fraction, density, and velocity of phase q, respectively.

The expression of balance of momentum for phase q is given as

$$\frac{\partial}{\partial t}\left(\alpha_q\rho_q\boldsymbol{u}_q\right)+\nabla\cdot\left(\alpha_q\rho_q\boldsymbol{u}_q\boldsymbol{u}_q\right)=-\alpha_q\nabla p+\nabla\cdot\boldsymbol{T}_q+\sum_{p=1}^{n}\left[K_{pq}\left(\boldsymbol{u}_p-\boldsymbol{u}_q\right)+\dot{m}_{pq}\boldsymbol{u}_{pq}\right]+\alpha_q\rho_q\left(\boldsymbol{F}_q+\boldsymbol{F}_{\text{lift},q}+\boldsymbol{F}_{\text{vm},q}\right) \tag{2}$$

where $\boldsymbol{T}_q$ is qth phase stress-strain tensor, which is computed by

$$\boldsymbol{T}_q=\alpha_q\mu_q\left(\nabla\boldsymbol{u}_q+\nabla\boldsymbol{u}_q^{\mathrm{T}}\right)+\partial_q\left(\lambda_q-\frac{2}{3}\mu_q\right)\nabla\cdot\boldsymbol{u}_q\boldsymbol{I} \tag{3}$$

Here, μ_q and λ_q are the shear and the bulk viscosity of phase q, respectively, $\boldsymbol{F}_q$ is an external body force, $\boldsymbol{F}_{\text{lift},q}$ is a lift force, $\boldsymbol{F}_{\text{vm},q}$ is a virtual mass force, K_{pq} is the interphase momentum exchange coefficient, $\dot{m}_{pq}$ characterizes the mass transfer from the pth to qth phase, and $\boldsymbol{u}_{pq}$ is the interphase velocity.

To describe the conservation of energy in the Eulerian multiphase applications, a separate enthalpy equation can be written for each phase by:

$$\frac{\partial}{\partial t}\left(\alpha_q\rho_q h_q\right)+\nabla\cdot\left(\alpha_q\rho_q\boldsymbol{u}_q h_q\right)=-\alpha_q\frac{\partial p_q}{\partial t}+\boldsymbol{T}_q:\nabla\boldsymbol{u}_q-\nabla\boldsymbol{q}_q+\sum_{p}^{n}\left(Q_{pq}+\dot{m}_{pq}h_{pq}\right) \tag{4}$$

where h_q is the specific enthalpy of the qth phase, $\boldsymbol{q}_q$ is the heat flux, Q_{pq} is the intensity of heat exchange between the pth and qth phases, and h_{pq} is the interphase enthalpy. The heat exchange between phases must comply with the local balance conditions $Q_{pq}=-Q_{qp}$ and $Q_{qq}=0$.

Velocity inlet boundary condition is used. Gas and particles are fully mixed before they enter the filter vessel. To simulate the back-pulse purge process, the boundary condition at the nozzle inlet is modified to a pressure boundary condition. The ceramic filters are treated as porous media with a given permeability and the penetration of the gas through the porous filter wall is computed as part of the solution. The permeability is decided by the Darcy law, which is given by [19]

$$\Delta p=-\frac{\mu}{k}v\delta \tag{5}$$

where Δp is seepage pressure drop, μ is gas molecular viscosity, which is a function of temperature, k is permeability, which is 1×10^{-12} m^2 in this simulation, v is filtration velocity of gas, δ is the thickness of the porous material.

The standard wall function is used in the simulation.

4 RESULTS AND DISCUSSION

First, the filtration process is simulated. The operation parameter is selected from an industry design

of ceramic filtration system. The gas velocity into the filter vessel is 7.05 $m \cdot s^{-1}$, with the operating pressure being 4.0 MPa, and the temperature being 673 K. In this model, the density of gas and particle are 22.4 and 2000 $kg \cdot m^{-3}$, respectively. The particle load is 10 $g \cdot m^{-3}$. The mean particle diameter is 3 μm. When the filtration process proceeds on for 300 s the boundary condition of nozzle corresponding to filter f3 and f4 are changed to pressure inlet from wall, so the pulse cleaning process begins. An average pressure of the pulse gas tank for the filter cleaning is 9.0 MPa at temperature 293 K. The pulse duration is 0.6 s.

4.1 Coupling effect between the gas and particles

Figure 3 shows the areal cake density distribution at the outside surface of filter f3 along the filter length at different circumferential position at $t = 240$ s and $t = 300$ s. The areal filter cake density increases from the close end of the filter and reaches the maximum at about the middle region, and then decreases when toward the top end of the candle filter. The distribution of the areal filter cake density along the filter length presents the similar trend at different circumferential position. It can be seen by comparing the areal filter cake density at different time that filter cake density increases more quickly at the region where the cake density is smaller. This is because the gas will enter the ceramic filter through the position with lower resistance, where the cake density is smaller and thereby more particles will settle on this place.

Figure 4 shows the radial velocity distribution at the outside surface of filter f3 (the distance is 0 mm from filter outside surface) along the filter length at time $t = 240$ s and $t = 300$ s. The radial velocity decreases from the close end of the filter and reaches the minimum of about 0.016 $m \cdot s^{-1}$ at about $z = 100$ mm,

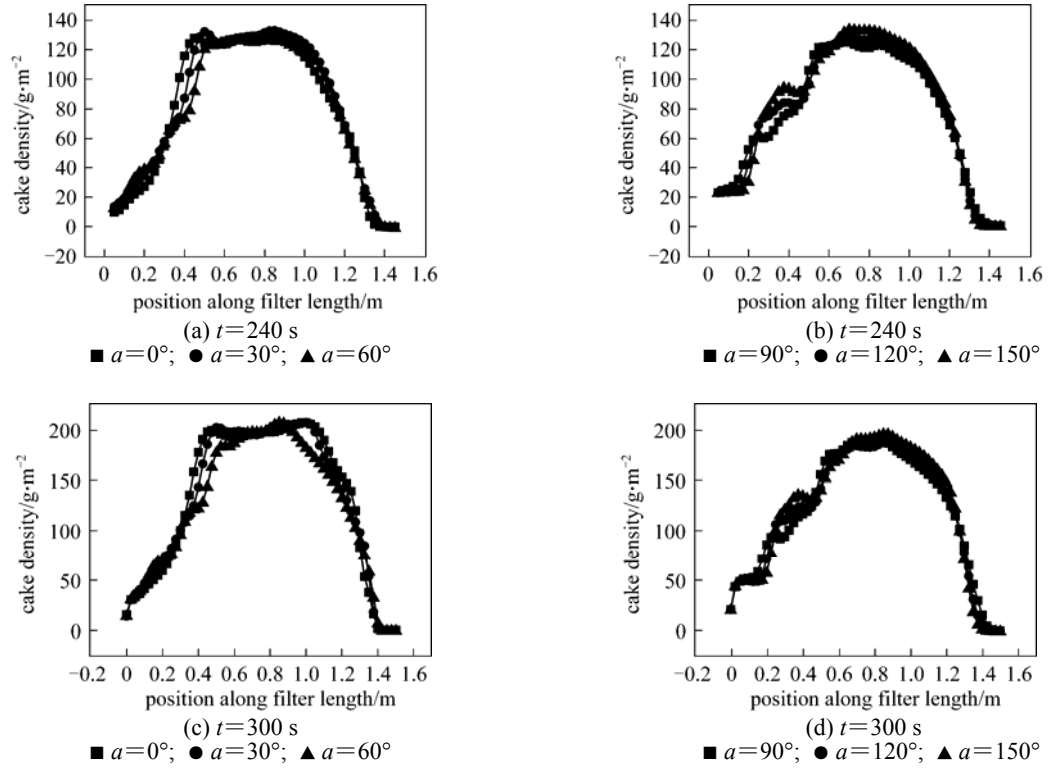

(a) t=240 s ■ a=0°; ● a=30°; ▲ a=60°

(b) t=240 s ■ a=90°; ● a=120°; ▲ a=150°

(c) t=300 s ■ a=0°; ● a=30°; ▲ a=60°

(d) t=300 s ■ a=90°; ● a=120°; ▲ a=150°

Figure 3 Variation of filter cake density on the surface of filter f3 with time along filter length

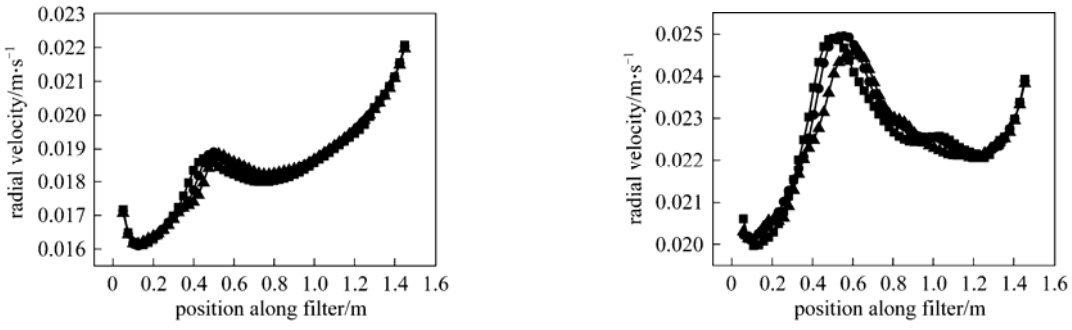

(a) t=240 s

(b) t=300 s

Figure 4 Variation of radial velocity outside filter f3 with time along filter length

■ a=0°; ● a=30°; ▲ a=60°

and increases along filter length reaching the maximum of about 0.019 $m \cdot s^{-1}$ ($t = 240$ s) at about $z = 800$ mm, and the decrease then toward the open end of the filter. The distribution of the radial velocity along the filter length shows the similar trend at different circumferential position and at different time with the only difference that the maximum radial velocity occurs to $z = 500$ mm at $t = 300$ s from top position at $t = 240$ s.

Comparison of Fig. 3 (c) with Fig. 4 (b) shows the interactional effect of the distribution of the areal

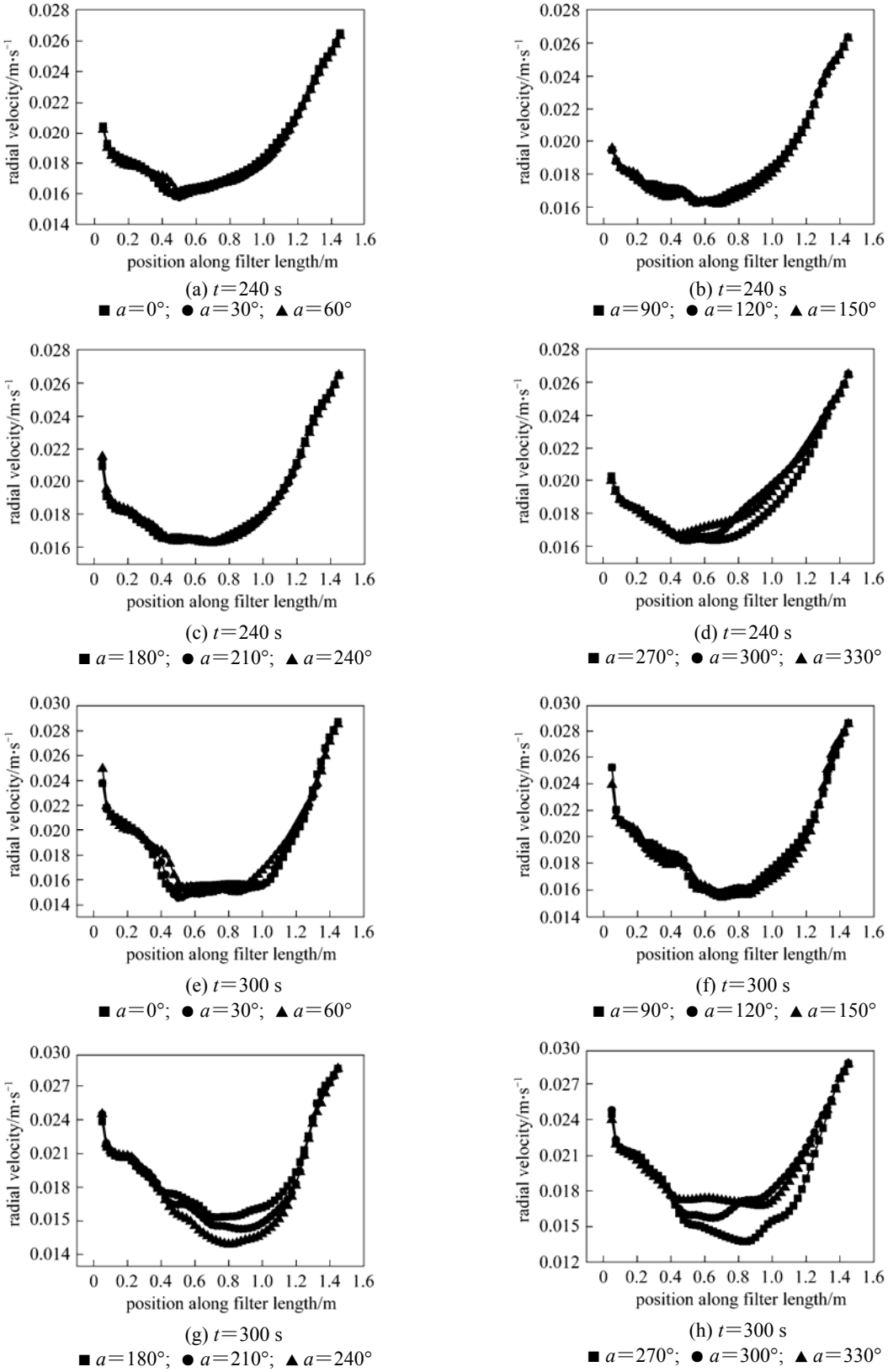

Figure 5 Variation of radial velocity in porous filter wall along filter length

cake density and gas radial velocity at the outside surface of filter f3 along the filter length at $t = 300$ s. The gas radial velocity is higher at the lower porosity region, where the filter cake density is higher. The filter cake density distribution along the filter is similar to that of gas radial velocity.

Figure 5 shows the variation of radial velocity distribution in porous media of filter f3 (the distance from filter outside surface is 5 mm) along the filter length. The gas flow distribution in porous media along filter length varies much when entering the candle filter. Gas radial velocity decreases upwards and reaches the minimum at about the middle region of the filter length, and increases then toward the top end of the filter. The distribution trend of radial velocity in the porous medium along the filter length is similar at different circumferential positions and at different times. The radial velocity decreases at the middle region and increases at the vicinity of the top and close end of the candle filter. More gas will enter filter from the upper and the lower region of the candle filter, and more particles will then deposited on these region on which the filter cake density will increase more quickly than that of on the middle region. Therefore the areal filter cake density distribution along the filter length will tend to be uniform with increase in filtration time.

Comparison of Fig. 3 (c) with Fig. 5 (e) shows interactional effect of the variation of the areal filter cake density and the gas radial velocity at the outside surface of filter f3 along filter length. The porosity is higher and accordingly the resistance is lower in the region, where the filter cake density is higher. Gas with particles will enter the filter at low resistance place so more particles will settle on this region.

Figure 6 shows the simulation result of pressure drop across the filter cake and the filter f3 element along the filter length at different times. The pressure drop increases from 2200 Pa at the bottom end to 3200 Pa at the top end of the filter at $t = 240$ s. Although the pressure drop changes from 3550 Pa at the bottom to 4000 Pa at the top part of the filter at $t = 300$ s, the pressure distribution along the filter length becomes more uniform with increase in the filtration time.

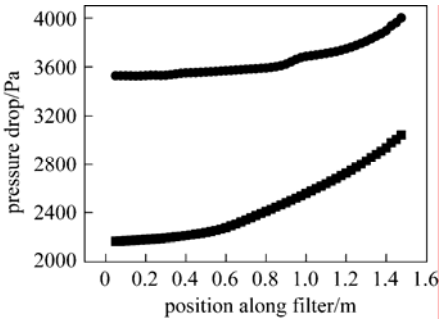

Figure 6 Variation of pressure drop across filter and filter cake along filter length
■ t=240 s; ● t=300 s

4.2 Effect of ongoing cleaning filter on normal filtration filter

Figure 7 is the areal filter cake density variation in the axial direction and the circumferential direction at the outside surface of the filter f2 (the distance from the filter outside surface is 0 mm) before/after the pulse cleaning process. Filter f2 acts as the role of filtration when its neighbor filter f4 is under cleaning. The filter cake density increases when the filtration

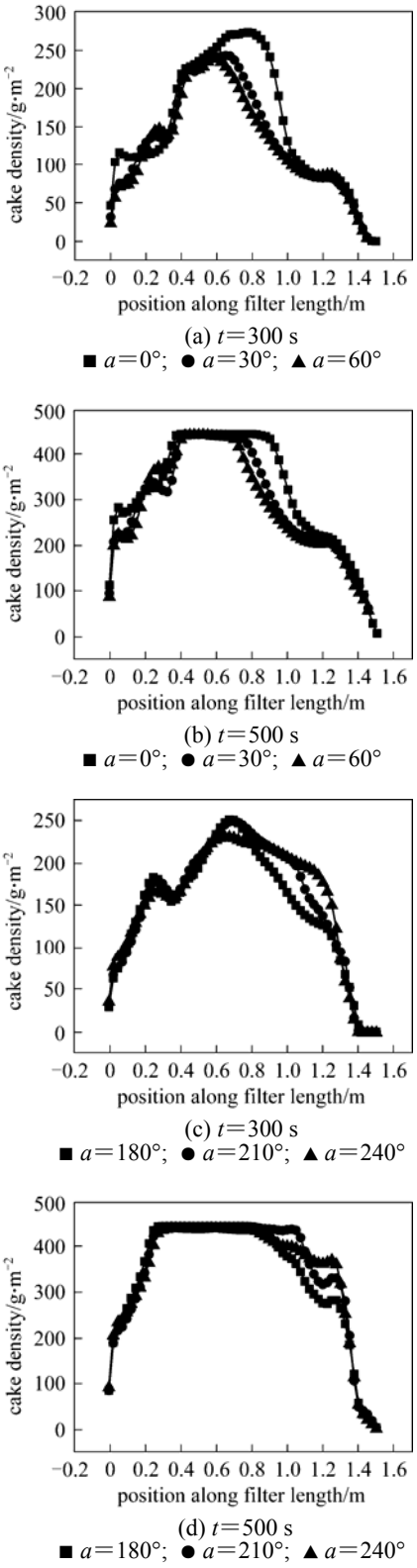

Figure 7 Variation of the filter cake outside the filter f2 along the filter length with time

process carries through. Figs. 7 (a) and (b) show that the filter cake density distribution along the filter length changes very little at the region of $a = 0-60°$ far from the cleaning filter f3. Figs. 7 (c) and (d) show that the filter cake density increase more quickly at the region of $a = 180°-240°$, which is adjacent to the cleaning filter f3.

5 CONCLUSIONS

A dense filter cake layer will form during the filtration process when gas carrying particle enters the ceramic filter element. The filter cake will affect the gas flow, and *vice versa* the gas flow pattern affects the particles movement. Areal filter cake density distribution is not uniform at the outside surface of filters at the early stage of filtration. Gas will encounter high resistance when it enters the ceramic filter element through the region with high cake density. So, more gas will enter the filter from low resistance place, where filter cake density is small and more particles will sediment on this region. Therefore, areal filter cake density distribution along the filter length will tend to be uniform with filtration process progressing.

The effect of pulse cleaning process on the filtration process is noticeable. Filter cake density at the outside surface of the filter f2 increases more quickly at the region, which is adjacent to cleaning filter f3.

NOMENCLATURE

a	angle, (°)
$\boldsymbol{F}_{\text{lift},q}$	lift force, N
$\boldsymbol{F}_q$	external body force, N
$\boldsymbol{F}_{\text{vm},q}$	virtual mass force, N
K_{pq}	interphase momentum exchange coefficient, kg·m^{-3}·s^{-1}
k	permeability, m^2
$\dot{m}_{pq}$	mass transfer from the pth to qth phase, kg·m^{-3}·s^{-1}
$\boldsymbol{T}_q$	stress-strain tensor of qth phase
t	time, s
$\boldsymbol{u}_q$	velocity of qth phase, m·s^{-1}
$\boldsymbol{u}_{pq}$	interphase velocity, m·s^{-1}
v	filtration velocity of gas, m·s^{-1}
z	height of the position from the origin of the coordinate system, mm
α_q	volume fraction of qth phase
δ	thickness of porous medium, m
λ_q	bulk viscosity of qth phase, Pa·s^{-1}
μ	molecular viscosity of the fluid, Pa·s^{-1}
μ_q	shear viscosity of qth phase, Pa·s^{-1}
ρ_q	density of qth phase, kg·m^{-3}

REFERENCES

1 Ji, Z.L., Shi, M.X., Ding, F.X., "Transient flow analysis of pulse-jet generating system in ceramic filter", *Powder Technol*., **139** (3), 200−207 (2004).
2 Fei, J.Y., Gao, T.Y., Yao, Y.P., Li, F., "Experimental study of filter flowing characteristics for candle ceramic filter elements", *J. Dalian Rallway Inst*., **27** (4), 31−34 (2006).
3 Schimidt, E., "Experimental investigations into the compression of dust cakes deposited on filter media", *Filtr. Sep*., **3**, 789−793 (1997).
4 Wu, J.H.,Wang, Y., " Study on an integrated sintered metal screen moving grannular bed filter", *Chin. J. Chem. Eng*., **12** (3), 458−462(2004).
5 Dittler, A., Ferer, M.V., Mathur, P., Djuranovic, P., "Patchy cleaning of rigid gas filters—transient regeneration phenomena comparison of modeling to experiment", *Powder Technol*., **124**, 55−66 (2002).
6 Smith, D.H., Powell, V., Ahamadi, G., Ibrahim, E., "Analysis of operational filtration data Part I. Ideal candle filter behavior", *Powder Technol*., **94**, 15−21 (1997).
7 Kamiya, H., Sekiya, Y., Horio, M., "Thermal stress fracture of rigid ceramic filter due to char combustion in collected dust layer on filter surface", *Powder Technol*., **115**, 139−145 (2001).
8 Kamiya, H., Deguchi, K., Gotou, J., "Increasing phenomena of pressure drop during dust removal using a rigid ceramic filter at high temperatures", *Powder Technol*., **118**, 160−165 (2001).
9 Filippova, O., Hänel, D., "Numerical simulation of particle deposition in filters", *J. Aerosol Sci*., **27**, 627−628 (1996).
10 Mugnier, N., Howell, J.A., Ruf, M., "Optimization of a back-flush sequence for zeolite microfiltration", *J. Membr. Sci*., **175**, 149−161 (2000).
11 Sasatsu, H., Misawa, N., Shimizu, M., Abe, R., "Predicting the pressure drop across hot gas filter (CTF) installed in a commercial size PFBC system", *Powder Technol*., **118**, 58−67 (2001).
12 Choi, J.H., Seo, Y.G., Chung, J.W., "Experimental study on the nozzle effect of the pulse cleaning for the ceramic filter candle", *Powder Technol*., **114**, 129−135 (2001).
13 Choi, J.H., Ha, S.J., Jang, H.J., "Compression properties of dust cake of fine fly ashes from a fluidized bed coal combustor on a ceramic filter", *Powder Technol*., **140**, 106−115(2004).
14 Li, H.X., Ji, Z.L., Wu, X.L., Choi, J.H., "Numerical analysis of flow field in the hot gas filter vessel during the pulse cleaning process", *Powder Technol*., **173**, 82−92 (2007).
15 Ji, Z.L., Jiao, H.Q., Chen, H.H., "Image analysis on detachment process of dust cake on ceramic candle filter", *Chin. J. Chem. Eng*., **13** (2), 178−183 (2005).
16 Dong, J.H., Wang, P., Xu, N.P., Shi, J., "Modeling of the relationship between pore size distribution and thickness of ceramic MF membrane", *Chin. J. Chem. Eng*., **6** (3), 178−183 (1998).
17 McCarthy, A.A., Walsh, P.K., Foley, G., "Experimental techniques for quantifying the cake mass, the cake and membrane resistances and the specific cake resistance during crossflow filtration of microbial suspensions", *J. Membr. Sci*., **201**, 31−45 (2002).
18 Zhang, X.W., Li, H., Yao, C.H., "Compressible gas flow in porous media/fluid coupled areas", *J. Chem. Ind. Eng*. (*China*), **54** (9), 1209−1214 (2003).
19 Jo, Y.M., Hutchison, R.B., Raper, J.A., "Characterization of ceramic composite membrane filters for hot gas cleaning", *Powder Technol*., **91**, 55−62 (1997).